Rainfall Estimation From TEMPEST-D CubeSat Observations: A Machine-Learning Approach

Chandrasekar Radhakrishnan, V. Chandrasekar, *Fellow, IEEE*, Steven C. Reising, *Senior Member, IEEE*, and Wesley Berg

***Abstract*—In this study, a machine-learning model was used to produce surface rainfall estimates from Temporal Experiment for Storms and Tropical Systems – Demonstration (TEMPEST-D) microwave radiance observations from a CubeSat. The machine-learning model is based on an artificial neural network (ANN). The space-borne TEMPEST-D sensor performed brightness temperature (TB) observations at five frequencies (i.e., 87, 164, 174, 178, and 181 GHz) during its nearly three-year mission. The TEMPEST-D TBs were used as inputs, and the multiradar/multisensor system (MRMS) radar-only quantitative precipitation estimation product at the surface was used as the ground truth to train the ANN model. A total of 19 storms were identified that were simultaneously observed by TEMPEST-D and ground weather radar over the contiguous United States. The training dataset used 14 of the 19 storm cases. The other five storm cases, consisting of three continental storms and two land-falling hurricanes, were used for independent testing. A spatial alignment algorithm was developed to align the TEMPEST-D observed storm with the ground radar measurement of the storm. This study showed that the TEMPEST-D TBs captured storm features as well as current-generation satellite sensors, such as the global precipitation mission microwave imager. The results of this study demonstrated that the rainfall estimated from TEMPEST-D matches well with the MRMS surface rainfall product in terms of rainfall intensity, area, and precipitation system pattern. The average structural similarity index measure score for the five independent test cases is 0.78.**

***Index Terms*—Artificial neural network (ANN), cubeSats, machine learning, multiradar/multisensor system (MRMS), quantitative precipitation estimation (QPE), smallsats, temporal experiment for storms and tropical systems – demonstration (TEMPEST-D).**

I. Introduction

THE accurate estimation of surface rainfall is essential for numerous weather and climate applications over both land and ocean. The knowledge of precipitation intensity and its spatiotemporal variability helps to understand the climatology of precipitation. In addition, precipitation is an essential global and climatic variable [1] and it is critical to systems that support life on earth. Over land, precipitation is a primary source of fresh water. Monitoring and measurement of precipitation patterns have substantial economic value for the agriculture and forestry [2]. Precipitation also plays a vital role in removing particulate matter from the atmosphere [3]. For these reasons, an extensive infrastructure of ground-based instruments (rain gauges [4] and weather radars [5]) and space-borne weather sensors [6] has been developed to accurately measure the spatiotemporal variability of precipitation on both regional and global scales. The significant spatial and temporal variability of precipitation makes it difficult to measure with high accuracy across multiple scales; dense observational networks are required to capture the variability of precipitation, particularly at fine spatial and temporal scales. Ground-based rain gauge networks collect direct measurements of surface rainfall and provide high temporal resolution observations. However, they provide insufficient spatial coverage to estimate rainfall over larger areas. Kidd *et al.* [7] reported that only 0.000000000593% of earth's surface is covered by ground-based rain gauges.

Ground-based weather radars form the key infrastructure to monitor storms, issue watches, and warnings, as well as provide data for numerical weather prediction (NWP). In addition to these benefits, weather radars provide precipitation estimates over large areas (7000–32 000 km^2) with high spatial and temporal resolution and reasonable accuracy at that scale. Ground-based weather radar networks are currently in use throughout the U.S. and some other parts of the world, providing accurate rainfall measurements within the radar network's area of coverage. However, current radar networks primarily observe rainfall over land. A limited number of radars also perform observations over coastal zones. Some limitations of ground-based weather radars are as follows: Rainfall products from weather radars have larger uncertainties over complex terrain; and they lack coverage over the oceans. Oceanic rainfall is essential for understanding the global water cycle as well as providing critical information to initialize NWP models for the accurate forecasting of severe weather events, such as hurricanes and tropical cyclones [8], [9].

Satellite-based precipitation observations can be used to provide global coverage, particularly over the ocean and in the polar regions. Currently, operational weather satellites are deployed in both geostationary orbit (GEO) and low earth orbit (LEO). Weather satellites in GEO orbits, approximately 36 000 km

Manuscript received December 30, 2021; revised February 27, 2022 and March 28, 2022; accepted April 12, 2022. Date of publication April 27, 2022; date of current version May 16, 2022. This work was supported by the NASA Earth Venture Technology Demonstration Program under Grant NNX15AP56G, Grant 80NSSC20K1124, and Grant 80NSSC21K2073 to Colorado State University. *(Corresponding author: Chandrasekar Radhakrishnan.)*

Chandrasekar Radhakrishnan is with the Cooperative Institute for Research in the Atmosphere, Colorado State University, Fort Collins, CO 80523 USA (e-mail: chandrasekar.radhakrishnan@colostate.edu).

V. Chandrasekar and Steven C. Reising are with the Department of Electrical and Computer Engineering, Colorado State University, Fort Collins, CO 80523 USA (e-mail: chandra@colostate.edu; steven.reising@colostate.edu).

Wesley Berg is with the Department of Atmospheric Science, Colorado State University, Fort Collins, CO 80523 USA (e-mail: wesley.berg@colostate.edu).

Digital Object Identifier 10.1109/JSTARS.2022.3170835

above the earth's surface, carry passive sensors to measure the atmosphere at visible (VIS), near-infrared (NIR), and infrared (IR) wavelengths. However, passive microwave sensors, with their longer wavelengths, are deployed only in LEO and not in GEO due to insufficient spatial resolution from GEO for reasonable real aperture sizes that can be launched into orbit. Synthetic aperture microwave radiometers have also been considered for GEO deployment but have not proven practical to date [10]. Geostationary satellites observe a large fixed area on the earth's surface and capture images with high temporal resolution. Surface rainfall products from VIS, NIR, and IR sensors in GEO are limited by the fact that these wavelengths provide very shallow penetration into clouds, increasing their uncertainty. For this reason, most surface rainfall estimation algorithms using GEO satellite observations are based only on cloud top brightness temperatures (TBs) [11]. These algorithms provide estimates over convective rainfall but are less suitable for stratiform and warm-top rainfall [12]. In contrast, passive microwave sensors in LEO provide improved estimates of surface rainfall with respect to GEO observations. The principal advantage over VIS, NIR, and IR sensors is that the passive microwave sensors penetrate clouds to respond to absorption and scattering from cloud particles and hydrometeors. At low microwave frequencies, radiometers respond principally to absorption and emission by water vapor and liquid water. At high microwave frequencies, radiometers additionally respond to scattering from solid hydrometeors, i.e., ice [13], [14]. Passive microwave observations also provide information about the vertical distribution of water vapor in the troposphere using pressure broadening of atmospheric absorption lines.

Studies are being conducted to develop machine-learning models to exploit the relationship between measurements by space-borne microwave sensors and precipitation products from ground radars. Many studies [15]–[17] conclude that including radar products greatly improves retrievals based only on passive microwave sensors. However, passive microwave sensors observing the atmosphere from LEO have long revisit times. Reducing revisit times requires the deployment and operation of a constellation of satellites [18]. However, such a deployment would be cost prohibitive using current-generation satellites. To provide a feasible solution, CubeSats provide a potential opportunity to build and launch a satellite constellation at dramatically lower cost [18]. As of January 1, 2021, more than 1200 CubeSats have been successfully deployed in LEO [19], including temporal experiment for storms and tropical systems – demonstration (TEMPEST-D). The rapid growth and development of CubeSat technology motivate the development of a model to retrieve surface rain rate from CubeSat observations. Therefore, this study focuses on developing a machine-learning model to estimate surface rain rate from TEMPEST-D CubeSat observations.

The rest of this article is organized as follows. Section II describes the TEMPEST-D mission and the concept of future 6U CubeSat constellations. Section III discusses the motivation to use TEMPEST-D observations to develop the rainfall estimation model and the methodology followed in the study. Section IV provides the details of the data collection and processing procedure to create the database to develop a machine-learning model. The artificial neural network (ANN) model development is described in Sections V and VI, including evaluation techniques used to determine the performance of the developed ANN model. In Section VII, the results are presented. Finally, Section VIII concludes this article.

Fig. 1. Image of TEMPEST-D satellite just after deployment from the International Space Station.

II. TEMPEST-D Satellite Mission

TEMPEST is a 6U CubeSat mission concept to observe the evolution of cloud convective systems with high temporal resolution. The TEMPEST constellation mission concept comprises 6–8 identical 6U CubeSats deployed in the same orbital plane with approximately 5-min spacing [20]. The TEMPEST-D ("D for demonstration") satellite is a single 6U CubeSat launched on May 21, 2018 and deployed into orbit on July 13, 2018. Fig. 1 shows the TEMPEST-D CubeSat on orbit shortly after deployment.

The TEMPEST-D radiometers measure at five millimeter-wave frequencies (87, 164, 174, 178, and 181 GHz) that provide detailed information on convection as well as the surrounding water vapor. A detailed description of the instrument and prelaunch calibration is provided in [21]. The TEMPEST-D mission performed continuous observations of the atmosphere for nearly three years. The radiometric performance of the TEMPEST-D instrument has been validated to be equivalent to on-orbit operational sensors on current-generation satellites, as discussed in [22]. TEMPEST-D has demonstrated the necessary technology for the success of the TEMPEST constellation, as illustrated in Fig. 2. Schulte *et al.* [23] used the TEMPEST-D TB observations to retrieve atmospheric water vapor, cloud liquid water path, and cloud ice water path. Their analysis showed that the retrieved products from TEMPEST-D agreed well with those obtained from the similar but more expensive and larger microwave humidity sounder sensors.

Fig. 3 shows TEMPEST-D observed storm events over three continents, along with the nearest-in-time global precipitation mission/global microwave imager (GPM-GMI) observations. The observations of the same storms by the two sensors look very similar. The top panel of the figure shows observations over south India on October 11, 2019, the middle panel shows observations over Africa on November 29, 2018, and the bottom

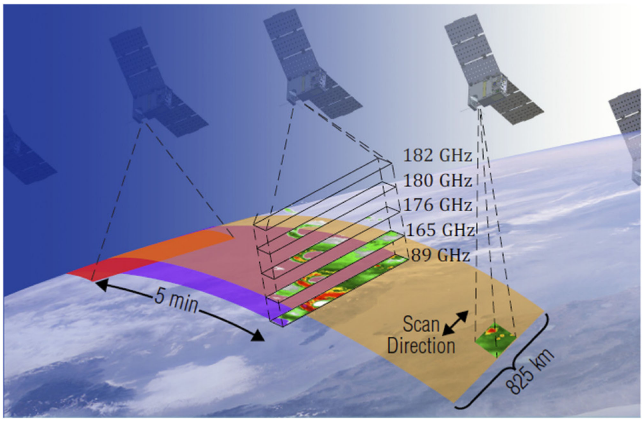

Fig. 2. Conceptual illustration of a TEMPEST CubeSat constellation.

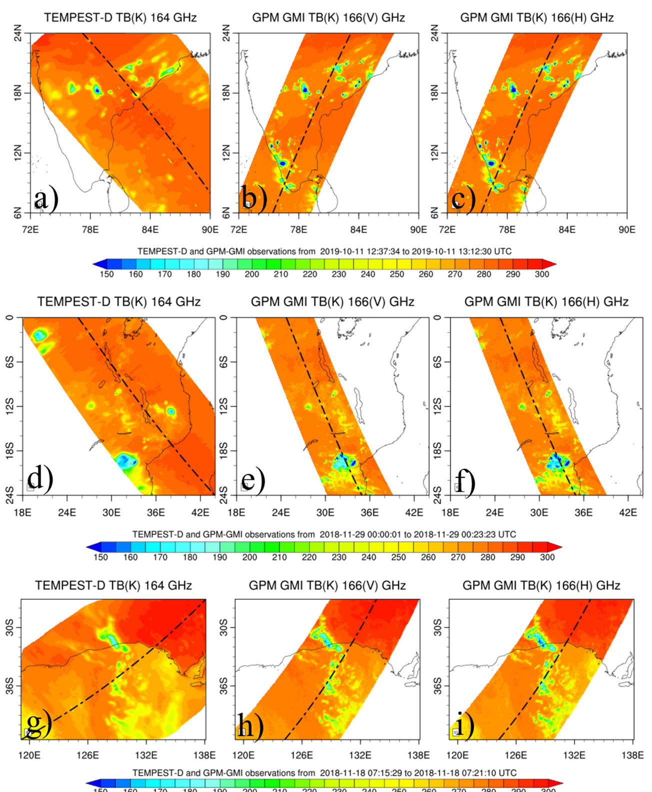

Fig. 3. Observations of storms over three continents by TEMPEST-D along with the nearest-in-time GPM-GMI observations. (a)–(c) Observations over southern India on October 11, 2019, from 12:37 to 13:12 UTC. (d)–(f) Observations over Africa on November 9, 2018, from 00:00 to 00:23 UTC. (g)–(i) Observations over Australia on November 18, 2018 from 07:15 to 07:21 UTC.

panel shows observations over Australia on November 18, 2018. Fig. 3 shows observations from the TEMPEST-D 164 GHz and the GPM-GMI 166 GHz vertical channels. Similar results were observed for the other TEMPEST-D channels.

III. Motivation and Methodology

Fig. 4 shows a comparison of TB observations from TEMPEST-D 164 GHz (a)–(c) with the corresponding nearest-in-time GPM-GMI 166 GHz vertical (d)–(f) channels over the Hurricane Dorian from August 30 to September 2, 2019. The hurricane structure and intensities observed by TEMPEST-D

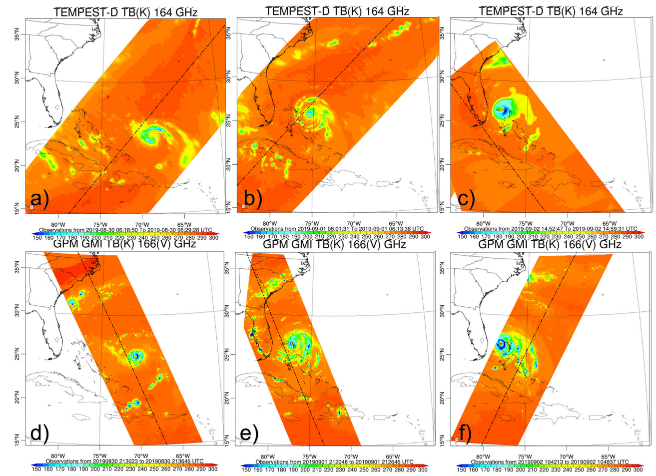

Fig. 4. Comparison of TEMPEST-D (a)–(c) with the corresponding nearest-in-time GPM-GMI (d)–(f) observations over Hurricane Dorian from August 30 to September 2, 2019.

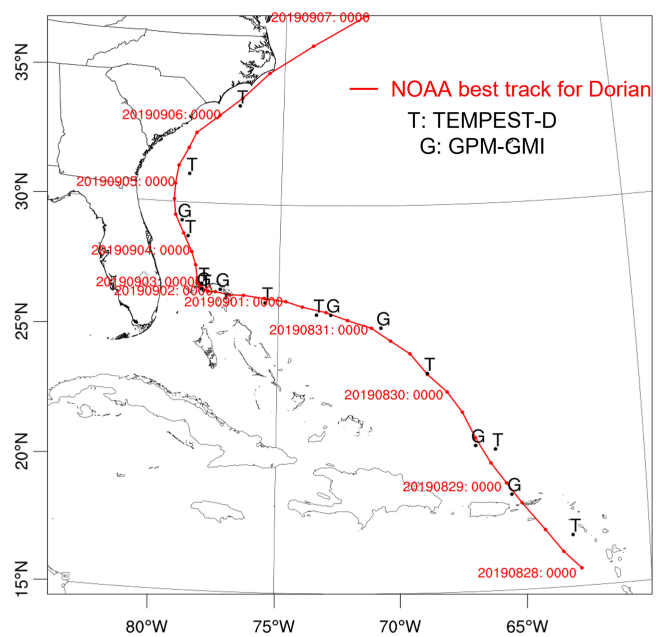

Fig. 5. Best track of Hurricane Dorian from NOAA along with locations of the hurricane's eye from TEMPEST-D and GPM-GMI observations. G refers to GPM-GMI and T refers to TEMPEST-D.

are similar to those observed by GPM-GMI, a more expensive current-generation satellite sensor. Fig. 4 shows the results from the TEMPEST-D 164 GHz channel; similar results were found for the other four channels.

Fig. 5 shows NOAAs best track of Hurricane Dorian along with the locations of the hurricane's eye from TEMPEST-D and GPM-GMI observations. It further shows that when considered together, TEMPEST-D and GPM-GMI provide more than twice the number of observations of Hurricane Dorian compared with observations from GPM-GMI only. This detailed comparison of TEMPEST-D and GPM-GMI observations for the case of Hurricane Dorian demonstrates that CubeSat observations can help to fill the gap between earth observations by current-generation LEO satellites. This potential coverage motivates further study to

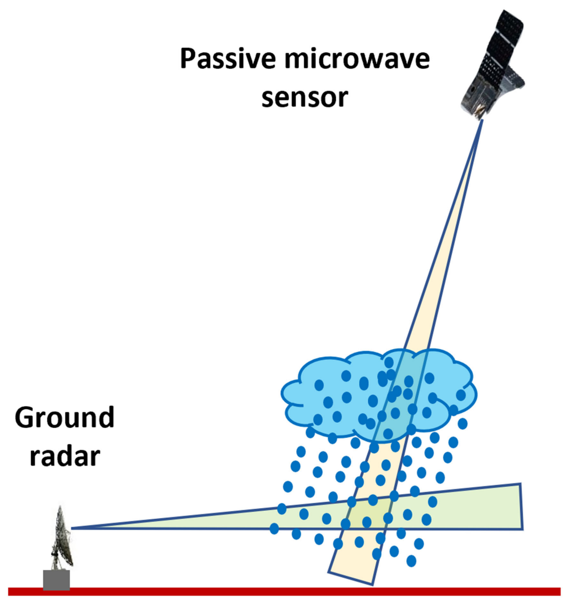

Fig. 6. Graphical representation of rainfall measurement from ground-based weather radar and a space-borne passive microwave sensor.

develop a model to estimate surface rainfall from CubeSats and merge it with rainfall products from current-generation satellites to improve global satellite-based rainfall products for a relatively low cost. Fig. 6 shows a conceptual diagram of simultaneous precipitation measurements from a ground-based weather radar and a space-borne passive microwave sensor. Weather radars directly measure the reflectivity of cloud particles and hydrometeors, which is converted into rainfall rate. Space-borne microwave radiometers capture upwelling radiation from the surface modified by atmospheric absorption and emission, including oxygen and water vapor. This radiation propagating through a cloud is then affected by absorption and emission by water droplets and scattered by ice particles. Therefore, the resulting TB measurements contain information about both clouds and both clouds and precipitation in the field of view of the radiometer. Since both active and passive microwave measurements provide information about clouds and precipitation, a machine-learning model can be developed to characterize the relationship between the two measurements. This study developed a machine-learning model in which the multiradar/multisensor system (MRMS) QPE rain rate product is considered as truth (target), and TB observations by the TEMPEST-D sensor at five frequencies are used as the predictor (input). The MRMS QPE products are generated at the NOAA National Severe Storms Laboratory (NSSL) in real time. The spatial resolution of the MRMS QPE product is 1 km, and the temporal resolution is 2 min. The NSSL integrates data from the nearly 165 *S*-band Doppler weather radars with current-generation satellite data and rain gauge observations to generate the MRMS QPE products over contiguous United States (CONUS) [24].

IV. Data Collection and Preprocessing

The first step is to identify each TEMPEST-D overpass observing storms within the CONUS region. The second step is to identify the MRMS surface rain rate product for the same storm corresponding to the TEMPEST-D observation identified in the first step. A total of 19 storm events were identified as being simultaneously observed by TEMPEST-D and MRMS. The radar quality index (RQI) [24] from MRMS has been used to assure the quality of MRMS QPE products for selected precipitation cases. The spatially averaged RQI for the storm events varies from 0.76 to 0.86. Two examples of TEMPEST-D channel TB observations and the corresponding MRMS QPE product are shown in Figs. 7 and 8. Fig. 7 shows a storm over the Gulf of Mexico and extending into Florida observed on June 9, 2019 at 08:12 UTC. Fig. 8 shows a storm over Arkansas and Texas observed on May 19, 2019 at 01:42 UTC. Fig. 9 shows the database creation process to develop the ML-based rainfall estimation model. The spatial resolution of the MRMS quantitative precipitation estimation (QPE) product is 1 km $\times$ 1 km. However, the TEMPEST-D spatial resolution is 25 km at nadir for 87 GHz and 12.5 km at nadir for the four frequencies near the 183.31 GHz water vapor absorption line. To accommodate this difference, in the final step of analysis, MRMS data are regridded to TEMPEST-D's spatial resolution.

Chandrasekar *et al.* [25] cross-validated coincident observations by TEMPEST-D and RainCube over precipitation systems and demonstrated that TEMPEST-D and RainCube observations of storms are highly correlated. Fig. 3 also shows very good agreement between coincident observations by TEMPEST-D and GPM-GMI over storms, in terms of storm location and time. These results demonstrate that TEMPEST-D has the capability to perform the observations of storms as well as current-generation research and operational space-borne sensors. However, the current study is focused on developing a machine-learning-based model to exploit the relationship between the ground-based weather radar estimated rain rate and TEMPEST-D TBs. This study utilizes coincident observations from two fundamentally different microwave remote sensing modalities, where NEXRAD is active and TEMPEST-D is passive. In addition, these two instruments observe storms using different scan patterns and frequencies. Careful consideration of these two datasets revealed a small spatial shift between the TEMPEST-D observations and MRMS precipitation estimates of storms. The analysis of all storm events demonstrated that the spatial shift between the two observations was less than 30–40 km. Such spatial shifts are small considering the differences between the space-borne and ground-based instrument characteristics. Previous studies [26], [27] also reported spatial misalignment when comparing observations from space-borne sensors and ground-based weather radars. They also developed algorithms to align the observations and performed quantitative cross comparisons [28], [29]. The application of the machine-learning model in this study requires a pixel-by-pixel comparison of TEMPEST-D observations with MRMS data. The shift is small, but it still needs to be corrected to ensure the efficacy of the machine-learning model, which depends on the correctness of the dataset used in the training phase.

Therefore, an alignment algorithm has been developed to correct the small spatial shift in TEMPEST-D observations to match the locations of the MRMS data. Fig. 10 shows a storm

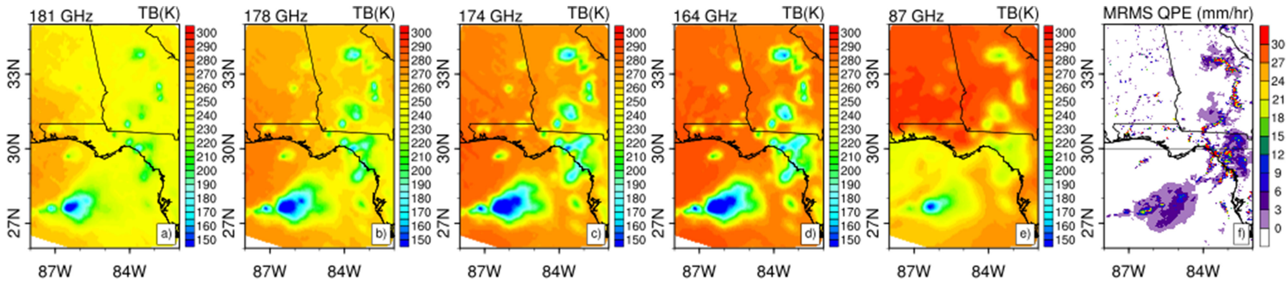

Fig. 7. TEMPEST-D observed TBs (a)–(e) and MRMS QPE (f) of a storm over the Gulf of Mexico and Florida on June 9, 2019 at 08:12 UTC.

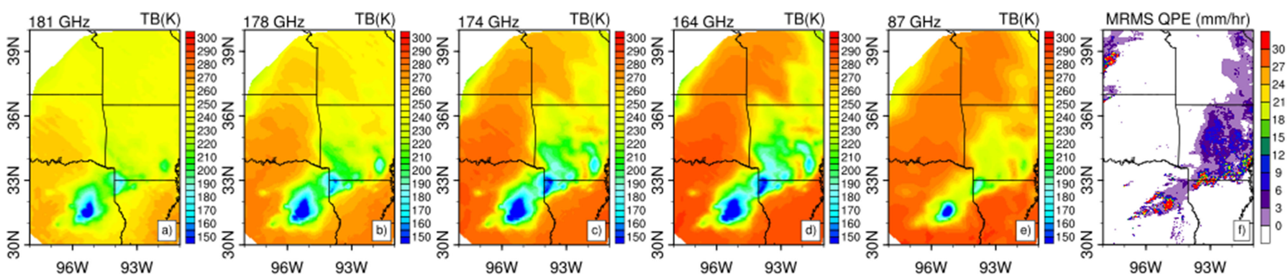

Fig. 8. TEMPEST-D observed TBs (a)–(e) and MRMS QPE (f) of a storm over Arkansas and Texas on May 19, 2019 at 01:42 UTC.

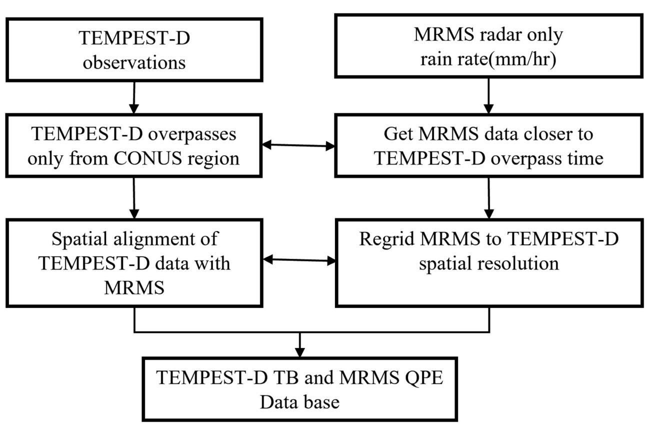

Fig. 9. Methodology to develop the ANN model for rainfall estimation.

observed by TEMPEST-D and MRMS on May 19, 2019, over Alto, Texas, before spatial alignment. Fig. 10(a)–(e) shows the observations from TEMPEST-D; Fig. 10(f) shows the MRMS QPE data regridded onto the TEMPEST-D grid; and Fig. 10(g) shows the MRMS QPE observation in the actual MRMS grid (1 km resolution). The black dotted contours in Fig. 10(a)–(e) show the 10 mm/hr precipitation rate isolines of the storm observed by MRMS. The solid red contours in Fig. 10(a)–(e) show the 130 K isolines of the TEMPEST-D observed TBs at each of the five frequencies. These isolines can be used to locate the center of the TEMPEST-D observed and MRMS estimated storms. The black dots show the center of each 10 mm/hr isoline contour from MRMS. The red dots show the centers of the 130 K isoline contours from TEMPEST-D observations. The contours show the horizontal shift between the two measurements. The alignment algorithm performs the random spatial

TABLE I
CORRELATION COEFFICIENT BETWEEN TEMPEST-D CHANNEL AND MRMS QPE PRODUCT FOR THE OBSERVATIONS SHOWN IN FIGS. 10 AND 11

Channels (GHz)	181	178	174	164	87
Before correction	-0.13	-0.15	-0.16	-0.17	-0.17
After correction	-0.72	-0.68	-0.65	-0.65	-0.74

shift in TEMPEST-D geo-coordinates to move the TEMPEST-D estimated storm center closer to the MRMS estimated storm center. The algorithm shifts the TEMPEST-D storm center to achieve maximum correlation with MRMS observations. A Pearson correlation coefficient is used to determine the effect of the spatial correction algorithm on TEMPEST-D data. Fig. 11 shows the same storm after spatial alignment. From Figs. 10 and 11, it is evident that the spatial alignment algorithm corrects the horizontal shift and that the two contours are well matched. Table I lists the correlations between the TEMPEST-D channel observations and the MRMS QPE products for the storm in Figs. 10 and 11, both before and after spatial correction. A negative correlation indicates that TEMPEST-D observed TBs and MRMS QPE are inversely correlated. Increasing surface rainfall is correlated with increases in ice scattering, leading to decreases in TBs. This storm case has the largest horizontal shift among the storm cases considered in this study. For this case, the horizontal shift was 38 km in longitude and 32 km in latitude. After alignment, the horizontal shift reduced to 3.1 km in longitude and 5.1 km in latitude.

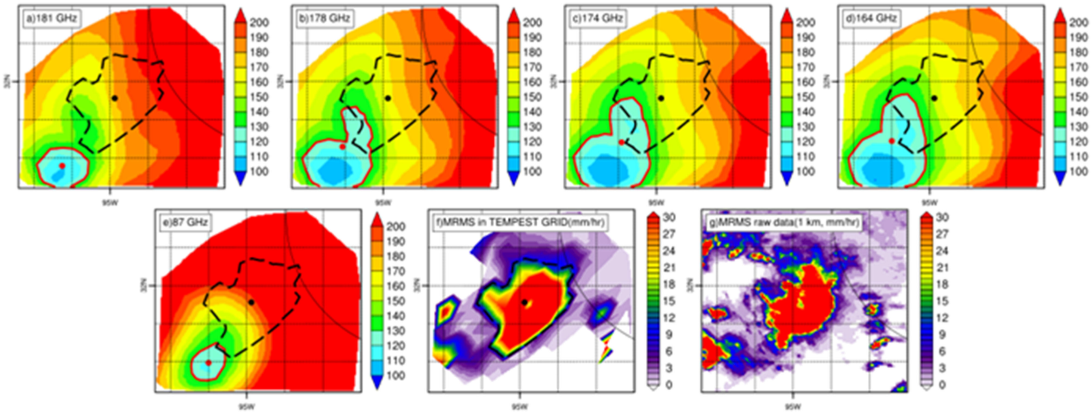

Fig. 10. TEMPEST-D observed TBs (a)–(e) of a storm on May 19, 2019 from 01:40 to 01:42 UTC over Alto, Texas, MRMS QPE at TEMPEST-D resolution, and (f) MRMS QPE at 1 km resolution (g) (before spatial correction).

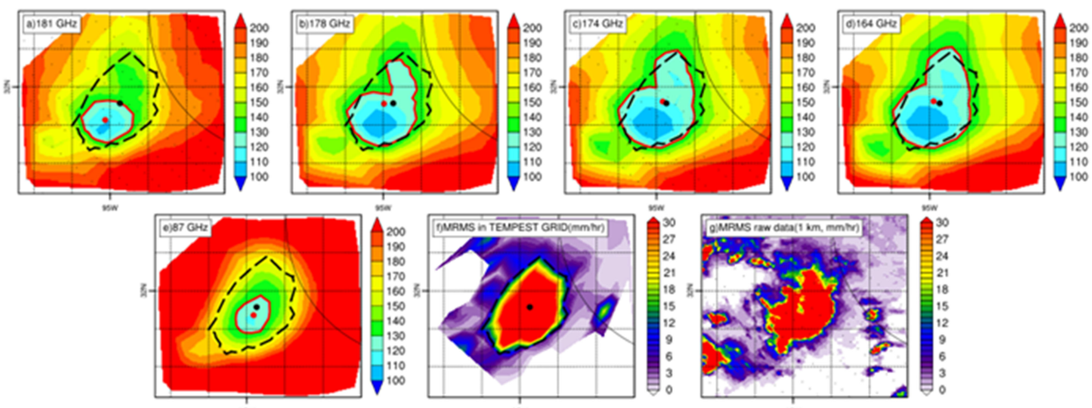

Fig. 11. TEMPEST-D observed TBs (a)–(e) of a storm on May 19, 2019 from 01:40 to 01:42 UTC over Alto, Texas, MRMS QPE at TEMPEST-D resolution, and (f) MRMS QPE at 1 km resolution (g) (after spatial correction).

V. ANN Model Development

ANN is a deep learning technique that is currently widely used in satellite remote sensing [30]–[32]. A fully connected feedforward and backpropagation neural network model was used in this study. A base dataset consisting of 14 storm cases was created to develop the model, and five storm events were used for independent testing. The base dataset consists of approximately 45 000 data points. The training dataset consists of 80% of the base dataset (36 000 data points), and the validation dataset consists of 20% of the base dataset (9000 data points). The independent test dataset consists of approximately 18 300 data points from five storm cases, including two land-falling hurricanes and three continental storms. The first step in ANN model development, a grid search experiment, was conducted to determine the optimum parameters for the base dataset. A grid search experiment has been conducted to determine the optimum set of hyperparameters for the ML model. Table II lists the names and ranges of the parameters used in the grid search experiment. Table III lists the optimum ANN parameters determined from the grid search and used in this study. Fig. 12 shows the best network determined from the grid study. The ANN network contains one input layer, three hidden layers, and one output layer. The input

TABLE II
Machine-Learning Parameters and Ranges for the Grid Search Experiment

	Parameter name	Range used in grid search
1	Optimizer	Adam, SGD, Adadelta
2	init mode	uniform, glorot_uniform, he_uniform
3	Activation function	relu, tanh, and sigmoid
4	Learning rate	0.001, 0.01, and 0.1
5	Hidden layers	2, 3, 4, 5, and 6
6	Number of neurons in hidden layer	6, 8, 10, 12, 14, and 16
7	Batch size	50, 75, 100, 125, 150
8	Epochs	20, 40, 60, 80, 100, 120

TABLE III
Parameters Used for Training the ANN

1	Optimizer	Adam
2	init mode	Glorot uniform initializer
3	Activation function	Rectified linear (ReLU)
4	Learning rate	0.01
5	Loss function	Mean Squared Error (MSE)
6	Batch size	100
7	Epochs	80

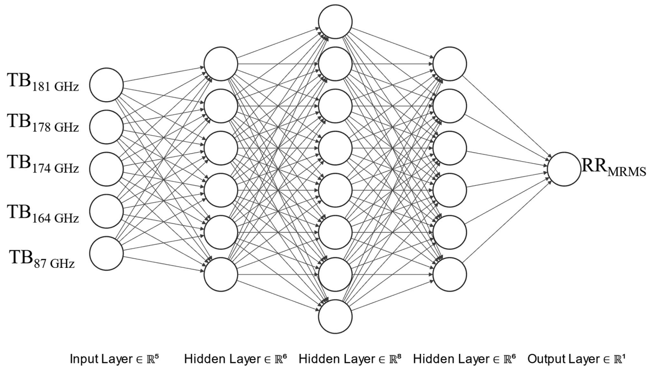

Fig. 12. ANN model structure adopted for rainfall estimation from TEMPEST-D TBs.

layers have five neurons, corresponding to TBs from each of the five TEMPEST-D channels. The output layer has one neuron, corresponding to MRMS retrieved rain rate. The three hidden layers have 6, 8, and 6 neurons, respectively.

VI. Evaluation Metrics

Even though the spatial correction algorithm can reduce uncertainty due to the different scan geometry and spatiotemporal mismatch between TEMPEST-D observations and MRMS QPE products, the fundamental physics of precipitation measurement differs between these two microwave instruments. NEXRAD radars are active and measure rain by reflection of raindrops and ice particles in the atmosphere. In contrast, TEMPEST-D radiometers are passive and measure the upwelling radiation from below, absorbed by water vapor and liquid water, as well as scattered by ice particles along the radiometer beam's path through the atmosphere. Therefore, it is very difficult to accurately estimate the precipitation rate for a specific pixel. Using an evaluation metric that mainly focuses on the pixel's rain rate intensity and performs a pixel-by-pixel comparison will underestimate the model's efficacy. For this reason, this study considers the TEMPEST-D estimated rain rate and MRMS QPE products as images and focuses on evaluating the consistency between them in terms of storm structure. This study evaluates the consistency of the TEMPEST-D estimated rain rate and the MRME QPE products using the structural similarity index measure (SSIM) metric. SSIM was proposed by Wang *et al.* [33] for measuring the similarity between two images and it is calculated as follows:

$$\mathrm{SSIM}_{x,y} = \frac{(2\mu_x\mu_y + C_1)(2\sigma_{xy} + C_2)}{(\mu_x^2 + \mu_y^2 + C_1)(\sigma_x^2 + \sigma_y^2 + C_2)} \qquad (1)$$

where μ_x and σ_x are the average and variance of x; μ_y and σ_y are the average and variance of y; σ_{xy} is the covariance of x and y; $C_1 = (K_1 L)^2$ and $C_2 = (K_2 L)^2$ are small positive constants that keep the denominator nonzero [34], L is the dynamic range of the pixel values (typically, this is 2 bits per pixel - 1); K_1 and K_2 are the scalar constants on the order of 0.01.

VII. Results and Discussion

The ANN model performance in rainfall estimation from the TEMPEST-D five-frequency TBs was evaluated using five independent storm events, including three storms over land and two land-falling hurricanes. Table IV lists the storm locations, dates, times, and SSIM scores. Figs. 13–17 show the TEMPEST-D observed TBs at all five frequencies, along with the TEMPEST-D estimated rainfall and MRMS QPE products. A spatial correction is applied to the TEMPEST-D observations for all five storm cases to reduce the spatial mismatch. Fig. 13 shows the observations of a storm over Fort Campbell, Kentucky, on October 7, 2019, at 01:06 UTC. Fig. 13(a)–(e) shows the TEMPEST-D TB observations. Fig. 13(f) shows the TEMPEST-D estimated rain rate; and Fig. 13(g) shows the MRMS QPE product. The figure clearly shows that the TEMPEST-D captured the storm that matched the ground radar observed storm in terms of storm location and structure. The estimated rain rate intensity also looks similar to the MRMS QPE products. The SSIM score is 0.72 between the TEMPEST-D estimated rainfall and the MRMS retrieved rainfall structure and location. This storm has two squall lines, and TEMPEST-D captured both squall lines, in agreement with ground-based radar observations.

Fig. 14 shows observations from a coastal storm near Wilmington, North Carolina, on November 17, 2019, at 07:00 UTC. Fig. 14(a)–(e) shows the TEMPEST-D TB observation, and Fig. 14(f) shows the corresponding rainfall estimation. Fig. 14(g) shows the MRMS QPE product over the same storm. This is an isolated storm near the coast. It was found that the storm features and structure look similar in both TEMPEST-D and ground radar observations. The TEMPEST-D TB from the 164 GHz channel [see Fig. 14(b)] captured the storm structure especially well. The shape and size of the intense inner part of the storm look similar in the TEMPEST-D estimated rain rate and MRMS QPE product. For this storm case, the SSIM score is 0.81 between the TEMPEST-D retrieved rainfall and the MRMS QPE rainfall. Fig. 15(a)–(e) shows the TEMPEST-D observations, along with the (f) TEMPEST-D estimated rain rate, and (g) MRMS QPE product from a Tropical Storm Olga over New Orleans, Louisiana on October 26, 2019, at 09:00 UTC. Tropical Storm Olga made landfall over central Louisiana in the early morning of October 26, 2019 and later moved across the Eastern United States to Ontario. It dissipated on October 28, 2019, and caused damage of over 400 million USD. TEMPEST-D observed Tropical Storm Olga just a few hours after it made landfall over New Orleans, Louisiana. The MRMS QPE product also showed heavy rainfall over the same area. Overall, the TEMPEST-D observation agreed well with the ground radar in terms of storm features and shape. This case shows one of the advantages of TEMPEST-D satellite observations over the ground-based radar. In the figure, the ground radar did not capture a small area of the storm over the ocean since it was outside of the area of ground radar coverage. However, TEMPEST-D can estimate the rain rate over the entire storm, a part of which is not covered by ground radar. Fig. 15(f) shows the intensity of the estimated rain rate from TEMPEST-D. It matches well with the MRMS QPE product, and the overall SSIM score for this case

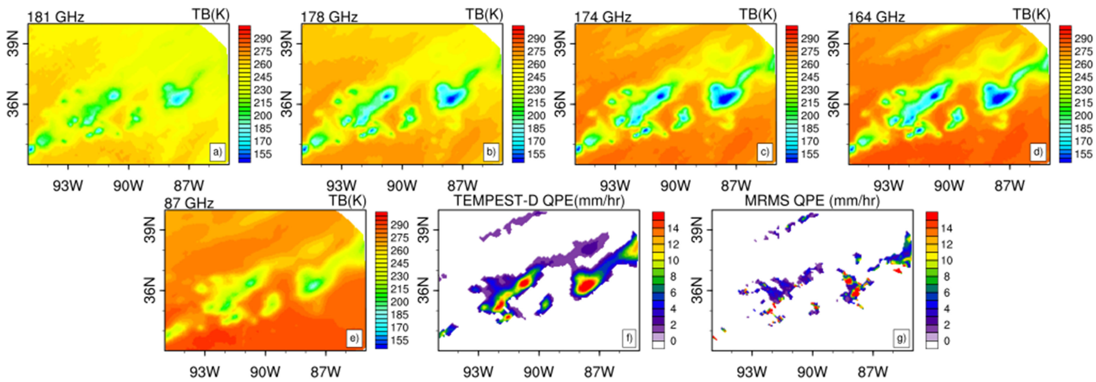

Fig. 13. (a)–(e) TEMPEST-D TB observations of a storm over Fort Campbell, Kentucky on October 7, 2019 at 01:06 UTC, (f) ANN estimated rain rate, and (g) MRMS rain rate.

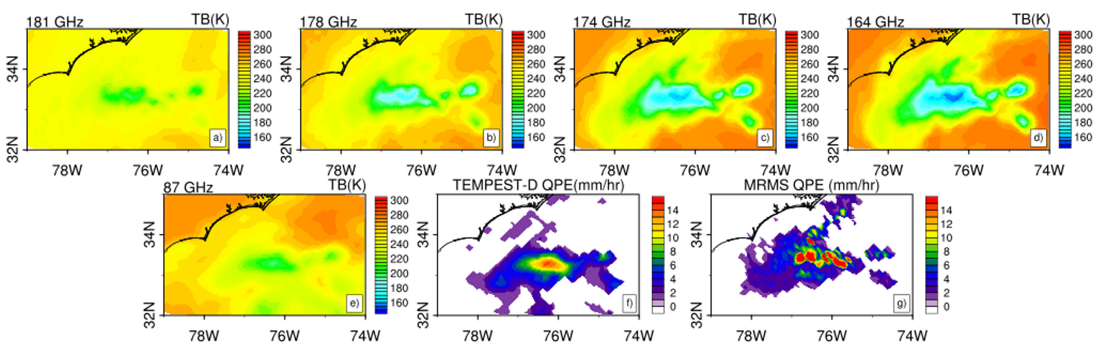

Fig. 14. (a)–(e) TEMPEST-D TB observations of a storm near Wilmington, North Carolina coast on November 17, 2019 at 07:00 UTC, (f) ANN estimated rain rate, and (g) MRMS rain rate.

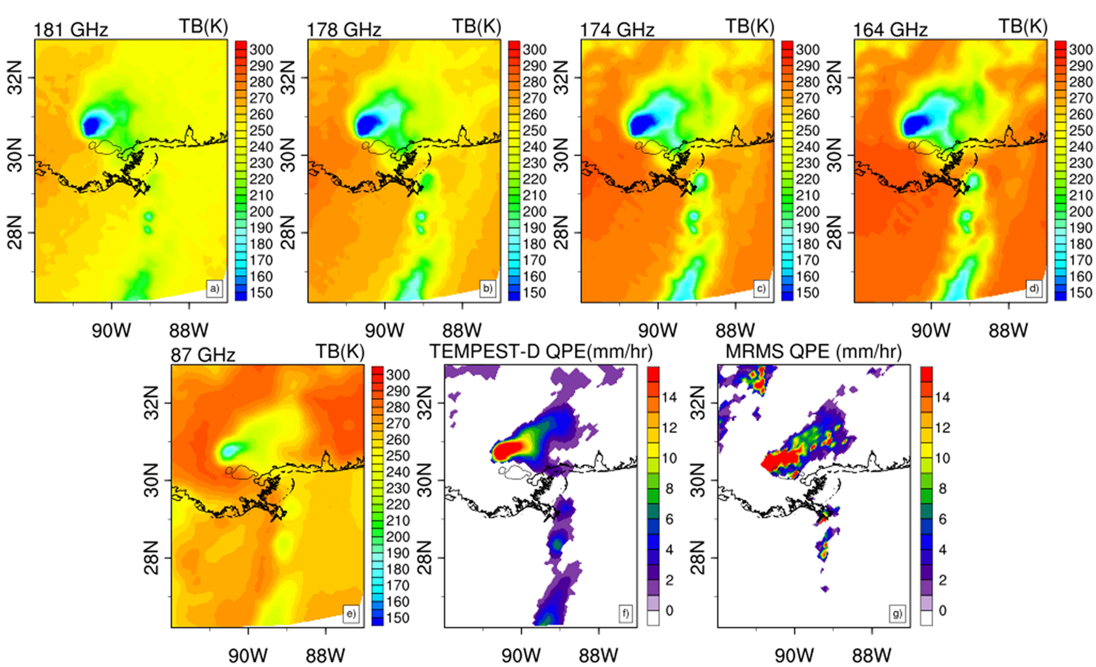

Fig. 15. (a)–(e) TEMPEST-D TB observations of Tropical Storm Olga over New Orleans, Louisiana on October 26, 2019 at 09:00 UTC, (f) TEMPEST-D estimated rain rate, and (g) MRMS rain rate.

TABLE IV
SSIM From Five Independent Storm Cases

	Storm event	Date and time	SSIM
1	Continental storm over Fort Campbell, Kentucky	Oct. 7, 2019, 01:06 UTC	0.72
2	Storm over Wilmington, North Carolina	Nov. 17, 2019, 07:00 UTC	0.81
3	Tropical Storm Olga over New Orleans, Louisiana	Oct. 26, 2019, 09:00 UTC	0.86
4	Hurricane Dorian over Grand Bahama Island	Sept. 2, 2019, 14:54 UTC	0.83
5	Storm near Florida costal area	Oct. 8, 2019, 15:00 UTC	0.70

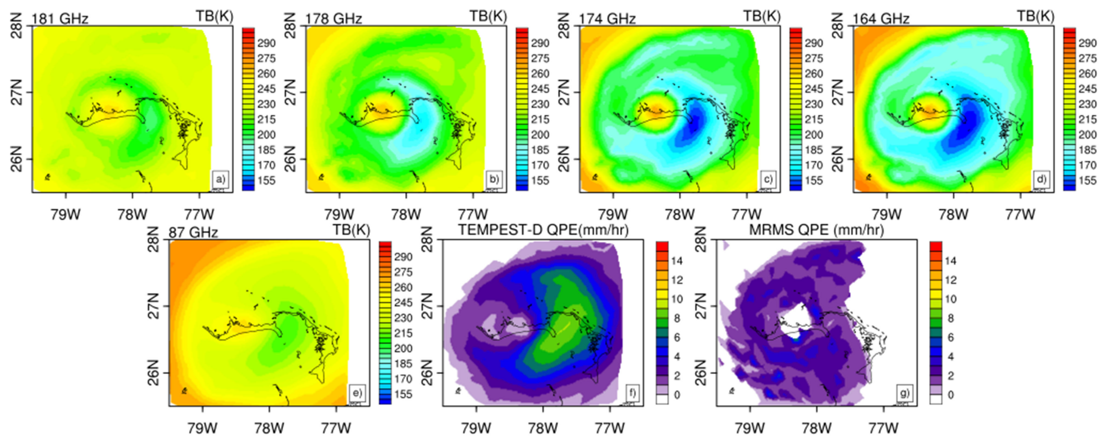

Fig. 16. (a)–(e) TEMPEST-D TB observations of Hurricane Dorian over Grand Bahama island on September 2, 2019 at 14:54 UTC, (f) TEMPEST-D estimated rain rate, and (g) MRMS QPE product.

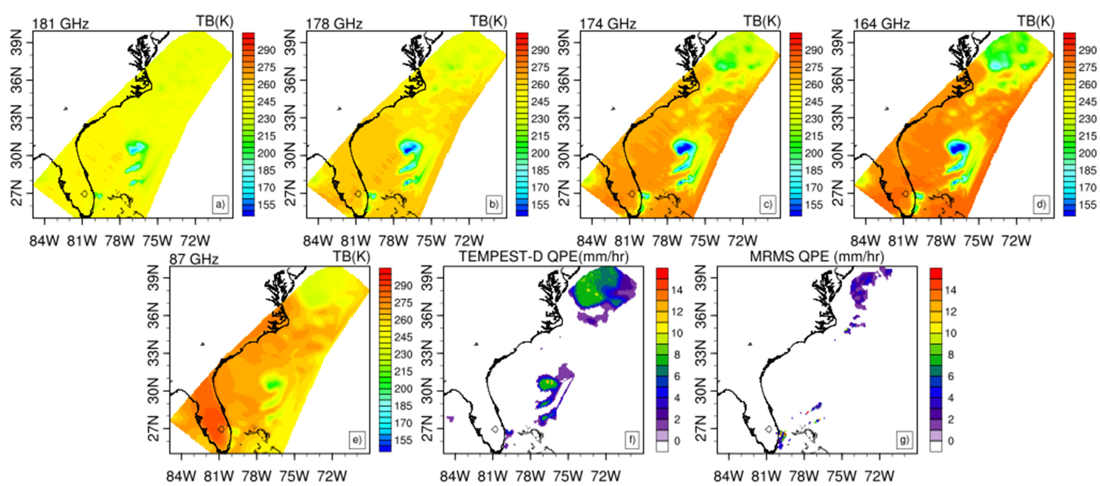

Fig. 17. (a)–(e) TEMPEST-D TB observations of a storm near Florida's Atlantic coast on October 8, 2019 at 15:00 UTC, (f) TEMPEST-D estimated rain rate, and (g) MRMS QPE.

is 0.86. Fig. 16(a)–(e) shows the TEMPEST-D TB observations, (f) TEMPEST-D retrieved rain rate, and the (g) MRMS QPE product from Hurricane Dorian over Grand Bahama Island on September 2, 2019, at 14:54 UTC. Hurricane Dorian was a Category 5 hurricane when it made landfall over Grand Bahama Island on September 1, 2019, at 16:40 UTC and caused damage of greater than 3.4 billion USD. TEMPEST-D captured Hurricane Dorian's rain bands on its outer edges, the eye, and the eyewall just after landfall. The TEMPEST-D estimated rain rate agrees well with MRMS QPE in terms of hurricane structure, and the SSIM score is 0.83. The TEMPEST-D retrieved rainfall intensity is greater than that of the MRMS QPE product. For this case, MRMS might underestimate the rain rate since, in this particular case, Hurricane Dorian is far from the NEXRAD radar network, which provides the primary input to generate MRMS QPE products. However, TEMPEST-D TBs at frequencies from 164 to 181 GHz show the heavy rain bands around the hurricane eyewall, which are missed in the MRMS QPE product. Fig. 17 shows observations from a storm near Florida's Atlantic coast on October 8, 2019, at 15:00 UTC. Fig. 17(a)–(e) shows the

TEMPEST-D TB observations, and Fig. 17(f) and (g) shows the TEMPEST-D estimated rain rate and MRMS QPE product, respectively. This case shows an advantage of TEMPEST-D over the ground radar network by its ability to capture the portion of the storm area that is not observed by ground radars. The SSIM score for this case is 0.7. The five independent test studies showed that TEMPEST-D channels could capture the storm and agreed well with the ground radar in terms of storm structure, area, and location. The developed ANN model has high efficacy in retrieving the surface rain rate from TEMPEST-D TBs. The retrieved rain rate agrees well with MRMS QPE products in terms of precipitation intensity and pattern.

VIII. Conclusion

A detailed investigation was performed to assess the capability of microwave TB observations from the TEMPEST-D CubeSat to observe storms over land and ocean. An ANN model is developed to estimate the surface rain rate from TEMPEST-D observations. The TEMPEST-D TBs at five frequencies are used as predictors, and the MRMS QPE product is used as the ground truth or target in the ANN model. A total of 19 storms were identified that were simultaneously observed by TEMPEST-D and ground weather radar over CONUS. A total of 14 storm cases were used to develop the ANN model, and five independent storm cases, including three continental storms and two land-falling hurricanes, were used for independent testing. The results of the evaluation demonstrated that the TEMPEST-D observations captured the storms in excellent agreement with the ground radar's observed storm location and structure. Also, the results showed that the TEMPEST-D microwave TB observations are as good as the observations from the more expensive current-generation satellites, such as GPM [22]. The independent test results showed that the TEMPEST-D estimated rain rate matched well with MRMS QPE products in terms of rain rate intensity, area, and pattern of precipitation system. The average SSIM score from the five independent storm cases is 0.78. This study presents the validation of a developed ML model over the CONUS region, where MRMS QPE products are available.

Acknowledgment

TEMPEST-D is a collaborative program with Caltech/NASA Jet Propulsion Laboratory and Blue Canyon Technologies. The authors would like to thank T. Gaier, S. Brown, S. Padmanabhan, and B. Lim of JPL for producing the TEMPEST-D radiometer instrument and providing calibrated geolocated brightness temperatures and P. Millar, G. Komar, B. Bauer, and S. Babu for their on-going support, encouragement, and program management.

References

[1] NASA Advisory Council, "Earth system sciences committee," Washington, DC, USA, 1988.
[2] R. H. Beach *et al.*, "Climate change impacts on US agriculture and forestry: Benefits of global climate stabilization," *Environ. Res. Lett.*, vol. 10, 2015, Art. no. 095004.
[3] J. Thornes *et al.*, "Communicating the value of atmospheric services," *Meteorol. Appl.*, vol. 17, no. 2, pp. 243–250, 2010.
[4] S. Tiwari, S. K. Jha, and A. Singh, "Quantification of node importance in rain gauge network: Influence of temporal resolution and rain gauge density," *Sci. Rep.*, vol. 10, 2020, Art. no. 9761.
[5] C. Radhakrishnan and V. Chandrasekar, "CASA prediction system over dallas–fort worth urban network: Blending of nowcasting and high-resolution numerical weather prediction model," *J. Atmos. Ocean. Technol.*, vol. 37, no. 2, pp. 211–228, 2020.
[6] G. Skofronick-Jackson *et al.*, "The global precipitation measurement (GPM) mission for science and society," *Bull. Amer. Meteorol. Soc.*, vol. 98, no. 8, pp. 1679–1695, 2017.
[7] C. Kidd *et al.*, "So, how much of the Earth's surface is covered by rain gauges?," *Bull. Amer. Meteorol. Soc.*, vol. 98, no. 1, pp. 69–78, 2017.
[8] R. Chandrasekar and C. Balaji, "Impact of physics parameterization and 3DVAR data assimilation on prediction of tropical cyclones in the Bay of Bengal region," *Natural Hazards*, vol. 80, no. 1, pp. 223–247, 2016.
[9] D. Subramani, R. Chandrasekar, K. S. Ramanujam, and C. Balaji, "A new ensemble-based data assimilation algorithm to improve track prediction of tropical cyclones," *Natural Hazards*, vol. 71, no. 1, pp. 659–682, 2014.
[10] A. B. Tanner *et al.*, "Initial results of the geostationary synthetic thinned array radiometer (GeoSTAR) demonstrator instrument," *IEEE Trans. Geosci. Remote Sens.*, vol. 45, no. 7, pp. 1947–1957, Jul. 2007.
[11] G. A. Vicente, R. A. Scofield, and W. P. Menzel, "The operational GOES infrared rainfall estimation technique," *Bull. Amer. Meteorol. Soc.*, vol. 79, no. 9, pp. 1883–1898, 1998.
[12] C. Kidd, D. R. Kniveton, M. C. Todd, and T. J. Bellerby, "Satellite rainfall estimation using combined passive microwave and infrared algorithms," *J. Hydrometeorol.*, vol. 4, no. 6, pp. 1088–1104, 2003.
[13] R. R. Ferraro *et al.*, "NOAA operational hydrological products derived from the advanced microwave sounding unit," *IEEE Trans. Geosci. Remote Sens.*, vol. 43, no. 5, pp. 1036–1049, May 2005.
[14] C. Kummerow *et al.*, "The evolution of the goddard profiling algorithm (GPROF) for rainfall estimation from passive microwave sensors," *J. Appl. Meteorol.*, vol. 40, no. 11, pp. 1801–1820, 2001.
[15] H. Chen, V. Chandrasekar, R. Cifelli, and P. Xie, "A machine learning system for precipitation estimation using satellite and ground radar network observations," *IEEE Trans. Geosci. Remote Sens.*, vol. 58, no. 2, pp. 982–994, Feb. 2020.
[16] Y. Derin *et al.*, "Passive microwave rainfall error analysis using high-resolution X-band dual-polarization radar observations in complex terrain," *IEEE Trans. Geosci. Remote Sens.*, vol. 56, no. 5, pp. 2565–2586, May 2018.
[17] V. Petkovic, M. Orescanin, P. Kirstetter, C. Kummerow, and R. Ferraro, "Enhancing PMW satellite precipitation estimation: Detecting convective class," *J. Atmos. Ocean. Technol.*, vol. 36, no. 12, pp. 2349–2363, 2019.
[18] Y. V. Goncharenko, W. Berg, S. C. Reising, F. Iturbide-Sanchez, and V. Chandrasekar, "Design and analysis of cubesat microwave radiometer constellations to observe temporal variability of the atmosphere," *IEEE J. Sel. Topics Appl. Earth Observ. Remote Sens.*, vol. 14, pp. 11728–11736, 2021, doi: 10.1109/JSTARS.2021.3128069.
[19] E. Kulu, "Nanosatellite & cubesat database." Accessed: Apr. 14, 2022. [Online]. Available: https://www.nanosats.eu/database
[20] S. C. Reising *et al.*, "An earth venture in-space technology demonstration mission for temporal experiment for storms and tropical systems (TEMPEST)," in *Proc. IEEE Int. Geosci. Remote Sens. Symp.*, 2018, pp. 6301–6303.
[21] S. Padmanabhan *et al.*, "TEMPEST-D radiometer: Instrument description and prelaunch calibration," *IEEE Trans. Geosci. Remote Sens.*, vol. 59, no. 12, pp. 10213–10226, Dec. 2021.
[22] W. Berg *et al.*, "Calibration and validation of the TEMPEST-D cubesat radiometer," *IEEE Trans. Geosci. Remote Sens.*, vol. 59, no. 6, pp. 4904–4914, Jun. 2021.
[23] R. M. Schulte *et al.*, "A passive microwave retrieval algorithm with minimal view-angle bias: Application to the TEMPEST-D cubesat mission," *J. Atmos. Ocean. Technol.*, vol. 37, no. 2, pp. 197–210, 2020.
[24] J. Zhang *et al.*, "Multi-radar multi-sensor (MRMS) quantitative precipitation estimation: Initial operating capabilities," *Bull. Amer. Meteorol. Soc.*, vol. 97, no. 4, pp. 621–638, 2016.
[25] V. Chandrasekar *et al.*, "Cross validation of TEMPEST-D and raincube observations," in *Proc. IEEE Int. Geosci. Remote Sens. Symp.*, 2021, pp. 7892–7895.
[26] S. M. Bolen and V. Chandrasekar, "Methodology for aligning and comparing spaceborne radar and ground-based radar observations," *J. Atmos. Ocean. Technol.*, vol. 20, no. 5, pp. 647–659, 2003.

[27] M. R. Schwaller and K. R. Morris, "A ground validation network for the global precipitation measurement mission," *J. Atmos. Ocean. Technol.*, vol. 28, no. 3, pp. 301–319, 2011.
[28] S. K. Biswas and V. Chandrasekar, "Cross-validation of observations between the GPM dual-frequency precipitation radar and ground based dual-polarization radars," *Remote Sens.*, vol. 10, no. 11, 2018, Art. no. 1773.
[29] Y. Ma, V. Chandrasekar, and S. K. Biswas, "A Bayesian correction approach for improving dual-frequency precipitation radar rainfall rate estimates," *J. Meteorol. Soc. Jpn., Ser. II*, vol. 98, no. 3, pp. 511–525, 2020.
[30] C. Balaji, C. Krishnamoorthy, and R. Chandrasekar, "On the possibility of retrieving near-surface rain rate from the microwave sounder SAPHIR of the megha-tropiques mission," *Curr. Sci.,* vol. 106, no. 4, pp. 587–593, 2014.
[31] S. R. Kannan, C. Radhakrishnan, and C. Balaji, "A new PCA-ANN algorithm for retrieval of rainfall structure in a precipitating atmosphere," *Int. J. Numer. Methods Heat Fluid Flow*, vol. 21, no. 8, pp. 1002–1025, 2011.
[32] S. Ramanujam, C. Radhakrishnan, D. Subramani, and B. Chakravarthy, "On the effect of non-raining parameters in retrieval of surface rain rate using TRMM PR and TMI measurements," *IEEE J. Sel. Topics Appl. Earth Observ. Remote Sens.*, vol. 5, no. 3, pp. 735–743, Jun. 2012.
[33] Z. Wang, A. C. Bovik, H. R. Sheikh, and E. P. Simoncelli, "Image quality assessment: From error visibility to structural similarity," *IEEE Trans. Image Process.*, vol. 13, no. 4, pp. 600–612, Apr. 2004.
[34] A. N. Avanaki, "Exact global histogram specification optimized for structural similarity," *Opt. Rev.*, vol. 16, pp. 613–621, 2009.

Chandrasekar Radhakrishnan received the bachelor's degree in mechanical engineering from Anna University, Chennai, India, in 2006, and the Ph.D. degree in mechanical engineering from IIT Madras, Chennai, India, in 2013.

He worked as a Research Scientist with IBM India Research Laboratory, New Delhi, India. He is currently working as a Research Scientist with the Cooperative Institute for Research in the Atmosphere, Colorado State University, Fort Collins, CO, USA. His interests include numerical weather prediction, data assimilation, satellite meteorology, radar-based nowcasting, and machine learning.

V. Chandrasekar (Fellow, IEEE) received the bachelor's degree in electrical engineering from IIT Kharagpur, Kharagpur, India, in 1981, and the Ph.D. degree in electrical engineering from Colorado State University (CSU), Fort Collins, CO, USA, in 1986.

He has also been the Director of the Research Experiences for Undergraduate Program for over 25 years, where he is involved in promoting research in the undergraduate curriculum. He is currently a University Distinguished Professor with CSU. He is also the Research Director of the National Science Foundation Engineering Research Center for Collaborative Adaptive Sensing of the Atmosphere. He has been actively involved in the research and development of weather radar systems for over 30 years. He has played a key role in developing the CSU-CHILL National Radar Facility as one of the most advanced meteorological radar systems available for research and continues to work actively with the CSU-CHILL radar, supporting its research and education mission. He is an avid experimentalist conducting special experiments to collect *in situ* observations to verify the new techniques and technologies. He has authored two textbooks and five general books and more than 250 peer-reviewed journal articles.

Dr. Chandrasekar is a Fellow of the American Meteorological Society, the American Geophysical Union, the International Union of Radio Science, and the National Oceanic and Atmospheric Administration (NOAA) Cooperative Institute for Research in the Atmosphere. He was a recipient of numerous awards, including Knighted by the Government of Finland, the NASA Technical Contribution Award, NASA Group Achievement Award, the NASA Robert H. Goddard Exceptional Achievement Award, the Outstanding Advisor Award, the IEEE GRSS Education Award, the NOAA/NWS Directors Medal of Excellence, and the IEEE GRSS Distinguished Achievement Award. He has served as the General Chair for the *IEEE International Geoscience and Remote Sensing Symposium* (IGARSS 2006).

Steven C. Reising (Senior Member, IEEE) received the B.S.E.E. (*magna cum laude*) and M.S.E.E. degrees from Washington University, St. Louis, MO, USA, in 1989 and 1991, respectively, and the Ph.D. degree from Stanford University, Stanford, CA, USA, in 1998, all in electrical engineering.

He served as an Assistant Professor of electrical and computer engineering with the University of Massachusetts Amherst, Amherst, MA, USA, where he received tenure. He served as a Summer Faculty Fellow for three summers with Remote Sensing Division, Naval Research Laboratory, Washington, DC, USA. In 2004, he joined Colorado State University, Fort Collins, CO, USA, where he served as an Associate Professor from August 2004 to June 2011 and has been a Full Professor of electrical and computer engineering since July 2011. His research interests span a broad range of remote sensing disciplines, including microwave remote sensing of the earth's atmosphere and oceans from airborne platforms, small satellites, and CubeSats; the design and development of radiometer systems from microwave to submillimeter-wave and THz frequencies (18–850 GHz); Lidar systems for sensing temperature and winds in the middle and upper atmosphere; and lightning–ionosphere interactions and atmospheric electrodynamics. He has been a Principal Investigator of 19 grants and contracts from NASA, NOAA, the National Science Foundation (NSF), the Office of Naval Research, National Polar-Orbiting Operational Environmental Satellite System Integrated Program Office, European Space Agency, Ball Aerospace, and FIRST RF. He has served as a Principal Faculty Advisor for 16 M.S./Ph.D. students who have completed their degrees and are currently employed as professors, engineers, and researchers in universities, industry, and government laboratories.

Dr. Reising was a recipient of the NSF CAREER Award (in the areas of physical and mesoscale dynamic meteorology) from 2003 to 2008, and the Office of Naval Research Young Investigator Program Award for passive microwave remote sensing of the oceans from 2000 to 2003. He currently serves as the Secretary of the IEEE Geoscience and Remote Sensing Society (GRSS, 2021-present). He previously served as the Chair of the Ad-hoc Committee for Intersocietal Relations (2019–2020) and as an elected Administrative Committee (AdCom) Member of the IEEE GRSS from 2003 to 2020. He also previously served as an elected AdCom Member of the IEEE Microwave Theory and Techniques Society (MTT-S) from 2014 to 2019. He served the IEEE as MTT-S Inter-Society Committee Chair from 2015 to 2018, GRSS Vice-President of Information Resources from 2011 to 2018, and the GRSS Vice-President of Technical Activities from 2008 to 2010. He was a founding member of IEEE GEOSCIENCE AND REMOTE SENSING LETTERS Editorial Board and served as an Associate Editor from 2004 to 2013. He is a Guest Editor of three Special Issues and one Special Section of IEEE TRANSACTIONS ON GEOSCIENCE AND REMOTE SENSING. He served as the Immediate Past Chair of the U.S. National Committee of the International Union of Radio Science (USNC-URSI) from 2015 to 2017, the Chair from 2012 to 2014, and the Secretary from 2009 to 2011, of all ten URSI Commissions. He is a member of URSI Commissions F, G, and H, the American Meteorological Society, the American Geophysical Union, the American Association for the Advancement of Science, Tau Beta Pi, and Eta Kappa Nu.

Wesley Berg received the B.S., M.S., and Ph.D. degrees in aerospace engineering from the University of Colorado, Boulder, CO, USA, in 1988, 1989, and 1993, respectively.

He worked with the Cooperative Institute for Research in Environmental Science, NOAA's Environmental Research Laboratories, Boulder, CO, USA. He is a Senior Research Scientist with the Department of Atmospheric Science, Colorado State University, Fort Collins, CO, USA. His research interests include satellite remote sensing of precipitation and other hydrologic parameters with a focus on instrument calibration and the development and analysis of satellite retrievals for long-term climate applications.